Journal of Materials Chemistry C

Accepted Manuscript

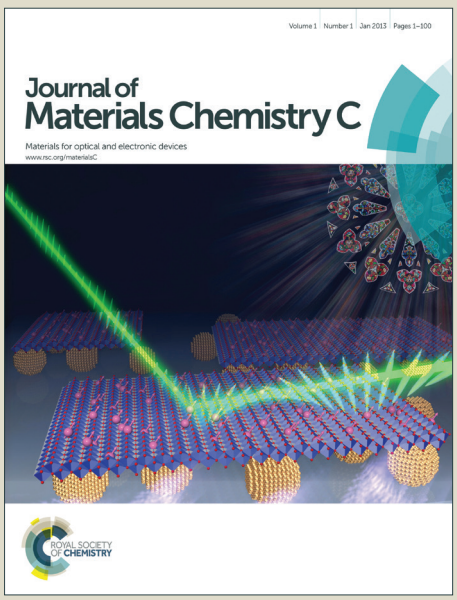

ROYAL SOCIETY OF CHEMISTRY

www.rsc.org/materialsC

Journal Name

ARTICLE

In situ iodoalkane-reduction of graphene oxide in polymer matrix: an easy and effective approach for the fabrication of conductive composites

Received 00th January 20xx,
Accepted 00th January 20xx

DOI: 10.1039/x0xx00000x

www.rsc.org/

Haiquan Guo,[*ab] Fangfang Liu, [ab] Jianying Zhao,[c] Haibo Yao,[a] Rizhe Jin,[a] Chuanqing Kang,[a] Zheng Bian,[a] Xuepeng Qiu,[a] Lianxun Gao[*a]

In situ chemical reduction (ISCR) of graphene oxide (GO) dispersed in polymer matrix has been regarded as an effective path to fabricate electrically conductive graphene/polymer composites due to the combination of perfect dispersion of GO in polymer matrix and high electrical conductivity of graphene. However, there are only very limited number of reducing agents that can be applied to ISCR process for the fabrication of graphene/polymer composites. Herein, we report an high-efficient reducing agent, 1,2-diiodoethane, which can be served to the preparation of graphene (IGO)/polyimide (PI) composites via ISCR process. The results showed that the electrical conductivity of IGO/PI composites with 2.5 wt% of IGO was 2.22 S m^{-1}, nearly seven orders of magnitudes higher than that of GO/PI without the addition of 1,2-diiodoethane. Moreover, the tensile strength and modulus of IGO/PI composites were increased by about 43% and 52% as compared with that of the pure PI, respectively. Furthermore, 1,2-diiodoethane and its decomposition products would not remain in the composites. The ISCR-based methodology can be extended to many other polymer composites and thus paves the way for easy and effective fabrication of conductive polymer composites.

1. Introduction

Ever since the isolation of free-standing graphene in 2004, the two-dimensional material consisting of a single layer of carbon atoms has been intensively investigated due to its remarkable mechanical, electrical, optical and thermal properties.[1-5] Graphene is a potential new material in various areas, covering optical and electronic devices, energy conversion and storage, biological and chemical sensors, polymer composites,[6-10] and so on. Especially, graphene sheets possess large specific surface area, great aspect ratio and outstanding electrical conductibility. Thus, graphene is an ideal candidate as conductive filler to fabricate conductive polymer composites that can be used for many technological fields,[11] such as electromagnetic shielding,[12, 13] flexible displays,[14] memory devices,[15] photovoltaic devices,[16] and electrochemical sensors,[17] etc. However, graphene tends to aggregate irreversibly owing to its high cohesive energy and strong π-π stacking interaction, which makes its exfoliation and incorporation into polymer matrix very difficult. As well known, the mechanical properties and electrical conductivity of graphene-based composites depend greatly on the dispersion level of graphene and the interfacial interaction between graphene and the polymer matrix. To improve the dispersion of graphene sheets in polymer matrix, one strategy suited to mass production is to use graphene oxide (GO) as a precursor to enhance compatibility with polymers.[18] Comparing with pristine graphene, GO bears many oxygen-containing functional groups on the basal planes and edges, which endows GO with excellent dispersity in polymer matrix. However, GO is electrically insulating. Therefore, for purpose of conductive fillers in polymer matrix, it is necessary to remove at least partially the oxygen functional groups and restore the conjugated carbon skeleton of graphene via reduction process. One of such processes is the chemical reduction of GO, which is a reliable route towards the large-scale production of graphene for commercial applications.

At present, there are a range of reducing agents reported in the literatures,[19] for example, hydrazine,[20] lithium aluminium hydride,[21] sodium borohydride,[22] hydroiodic acid,[23] ferric iodide/hydrochloric acid,[24] and potassium iodide/hydrochloric acid.[25, 26] Although these reducing agents can produce high reduction extent graphene, the irreversible aggregation of the produced graphene is often observed during chemical reduction of GO, which affects remarkably the construction efficiency of conductive networks in polymer matrix and thus affords unsatisfactory electrical conductivity for composites. Recently, the so-called *in situ* chemical reduction (ISCR) of GO dispersed in polymer matrix has attracted considerable attentions.[27] ISCR offers a simple and effective fabrication

[a] State Key Laboratory of Polymer Physics and Chemistry, Changchun Institute of Applied Chemistry, Chinese Academy of Sciences, Changchun 130022, China. E-mail: lxgao@ciac.ac.cn.
[b] University of Chinese Academy of Sciences, Beijing 100039, China. E-mail: hqguo@ciac.ac.cn.
[c] College of Chemical Engineering, Shandong University of Technology, Zibo 255049, China.

procedure of conductive polymer composites, which involves dispersion of GO in polymer matrix followed by chemical reduction during composites process. The strategy can prevent restacking and aggregation of reduced GO sheets during reduction process. ISCR holds great potential to be developed as a cost-effective and commercially viable process to produce conductive composites. Recently, Wang *et al.* had demonstrated that GO dispersed in poly(vinylidene fluoride) matrix could be reduced *in situ* by phenylhydrazine.[28] Similarly, the reduction of GO dispersed in epoxy resin using hydrazine had been reported by Kim *et al.*[29] In another study, Ku *et al.* suggested that GO functionalized with 4-iodoaniline could be *in situ* thermo-chemically reduced in polyimide (PI) matrix at 430 ^{o}C, and the electrical conductivity of the composite with 10 wt% graphene was 0.87 S m^{-1}.[30] Other researchers have also paid attention to the synthesis of graphene/phenol formaldehyde resin (PF) composites because phenol acts both as monomer of PF and reducing agent of the GO.[31, 32] Although a few reducing agents have been used for *in situ* chemical reduction of GO in polymer matrix, most of them are only suitable for specific polymers.[33] Moreover, some reducing agents are not only harmful to both human health and the environment but also unsuitable for most polymers since the possible reaction between these reducing agents and polymers may destroy the polymer structures. In addition, the residual reducing agents may also impact the properties of the graphene/polymer composites. At present, the electrical conductivity of the composites via the ISCR process was still insufficient for many practical applications. Therefore, it is necessary to develop new efficient chemical reducing agents for the *in situ* preparation of graphene/polymer composites with high conductivity, mechanical properties and no residue.

In this work, we reported a new reducing agent, 1,2-diiodoethane, which was applied to the fabrication of polyimide-based composites via the ISCR process. The fabrication methodology involved two basic processes: the preparation of the GO/ polyamide acid (PAA, the precursor of PI) solution via *in situ* polymerization and the fabrication of the composite films through heating process during which GO was reduced *in situ* to graphene (IGO) by 1,2-diiodoethane. The method combining *in situ* polymerization and *in situ* reduction took full advantage of dispersibility of GO and conductibility of IGO, hence the composite films have high conductivity and improved mechanical performances.

2. Experimental

2.1. Materials

Flake Graphite (100 mesh) was purchased from Shanghai Daoguan Chemical Factory (China). 1,2-Diiodoethane was supplied by Alfa Aesar. Potassium permanganate (AR), sulfuric acid (98 wt%), hydrochloric acid (36–38 wt%), and hydrogen peroxide (30 wt%) were purchase from Fuyu Chemical Factory (China). 3,3',4,4'-Biphenyl tertracarboxylic dianhydride (BPDA) was supplied from Shijiazhuang Haili Fine-Chemical Co., Ltd.. 4,4'-Oxydianiline (ODA) was obtained from Wanda Chemical Group. *N,N*-dimethylacetamide (DMAc) was obtained from Tianjin Reagent Co., Ltd. and distilled over CaH_2 under reduced pressure. All the other reagents were used as received unless specified.

2.2. Reduction of graphene oxide by 1,2-diiodoethane

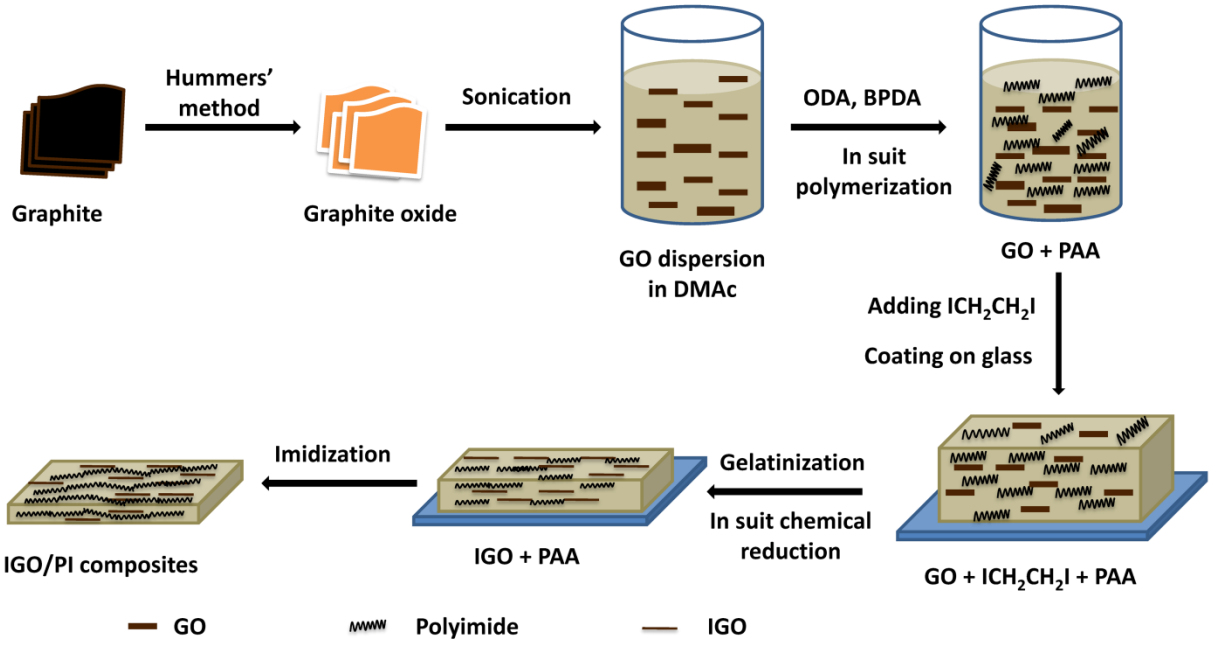

Fig. 1 Scheme of the preparation procedure for IGO/PI composite films.

Graphene oxide (GO) was prepared from flake graphite through a modified Hummers' method.[34] In brief, flake graphite (2 g) was added into H_2SO_4 (40 mL) and stirred for 2 h while adding $KMnO_4$ (12 g) gradually to keep the temperature of the solution at 30-40 °C. The resulting mixture was then stirred at 40 °C for 30 min and then at 80 °C for 2 h. H_2O (200 mL) was slowly dropped into the resulting solution, over a period of around 60 min. It was observed that the temperature rapidly increase to 95 °C. The reaction was quenched by adding H_2O_2 solution (30%, aqueous solution 3 mL). The diluted suspension was washed with HCl (5% aqueous solution) and deionized water by centrifugation, respectively, until the pH value became neutral. The light brown graphite oxide was collected and dried under vacuum. The exfoliation of graphite oxide to GO was carried out by ultrasonic dispersion in DMAc. Graphite oxide (500 mg) was dispersed in DMAc (200 mL) by ultrasound cleaner to create a brown dispersion and then centrifuged to remove any unexfoliated GO.

1,2-Diiodoethane (20 mg) was added into the homogeneous GO dispersion in DMAc (0.4 mg/mL, 5 mL), followed by heating at 80°C for different times. As the reaction progressed, the clear, brown GO dispersion gradually turned hazy, and eventually the black slurry were observed inside the reaction vessel. The resulting precipitates were filtrated, and washed with ethyl alcohol (50 mL) four times. The as-prepared product was dried under vacuum, and the black powder of IGO was obtained. In order to investigate the conversion from GO to IGO, the reaction time was varied from 2 h to 12 h. The corresponding IGO was denoted as IGO-2h, IGO-4h, IGO-6h, and IGO-12h, respectively.

2.3. Preparation of IGO/PI composite films and GO/PI composite films

IGO/PI composite film with 1.0 wt% IGO was prepared as follows (Fig. 1): the homogeneous GO dispersion (2 mg/mL, 25 mL) in DMAc were charged into three-necked flask equipped with a mechanical stirrer and nitrogen inlet and outlet. Then, ODA (2.00 g, 0.01 mol) was added to the mixture and stirred for 1 h, followed by the addition of BPDA (2.94 g, 0.01 mol). The mixture was stirred for 12 h at 0 °C, affording GO/PAA solution. To the GO/PAA solution 1,2-diiodoethane (0.5 g) was added, and subsequently, the viscous solution was casted on the glass substrate, followed by thermal imidizaton at 80°C for 5 h, and then at 150, 200, 250, 300 and 350°C each for 0.5 h to obtain 1.0 wt% IGO/PI composite. The content of IGO in the composites was based on the addition of GO. The free-standing IGO/PI film was peeled from the substrate by immersing in hot water at 60 °C for about 4 h. Other specimens (0.5 wt% IGO/PI, 1.5 wt% IGO/PI, 2.0 wt% IGO/PI, and 2.5 wt% IGO/PI) containing 0.5 wt%, 1.5 wt%, 2.0 wt%, and 2.5 wt% of IGO were also prepared by the above-mentioned experimental steps. For comparison, the GO/PI composite films were fabricated in the similar manner without the addition of 1,2-diiodoethane. The thicknesses of obtained composite films varied between 40 and 50 μm.

2.4. Characterization

UV-visible spectra of dilute aqueous solution of GO and IGO after ultrasonication were obtained using a UV-2550 Shimadzu UV-visible spectrophotometer. Fourier transform infrared (FTIR) spectroscopy was performed at room temperature using a Bruker Vertex 70 FTIR spectrometer. X-ray diffraction (XRD) analysis was carried out on a Bruker D8 Advance x-ray multicrystal diffraction spectrometer equipped with Cu Kα radiation of wavelength λ= 0.1541 nm and operated at 200 mA and 40 kV. X-ray photoelectron spectroscopy (XPS) spectrum was recorded using an ESCALab250 electron spectrometer from Thermo Scientific Corporation with monochromatic Al Kα radiations. Raman spectra was excited with a laser of 532 nm and recorded on a BTR111MiniRam Raman spectrometer. Microscopic morphology observations were conducted on a high resolution transmission electron microscopic (FEI Tecnai G2 F20 S-TWIN) working at 200kV. The facture surface morphology of the composite films was investigated by XL30 ESEM FEG field emission scanning electron microscope (SEM) under an acceleration voltage of 5 kV. Mechanical properties of films were examined at room temperature on a INSTRON-1121 universal testing apparatus with a crosshead speed of 5 mm min^{-1}; Young's modulus and maximum tensile strength were calculated as the average of at least five specimens. The electrical conductivities of IGO and the composite films were measured based on a four-point probe mode using a resistivity measurement system (Keithley 2182 nanovoltmeter and Keithley 2400 source meter).

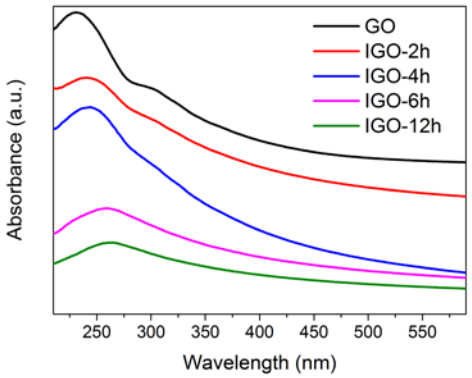

Fig. 2 UV-Vis spectra of GO and IGO with different reduction times.

3. Results and discussion

3.1. Spectral studies of GO and IGO

In order to monitor the entire reaction process during which GO was reduced by 1,2-diiodoethane in DMAc at 80 °C, the time-dependent UV–Vis spectra were recorded(Fig. 2). GO exhibits a maximum absorption at 231 nm and a weak shoulder peak at about 300 nm, which corresponds to the π-π* transitions of aromatic C=C bonds and the n-π* transitions of the C=O bonds in GO, respectively.[35] After reduction, the absorption peak at 231 nm originating from the π-π* transitions of the C=C bonds gradually red-shifted to ~240, 244, 258 and 264 nm by increasing the reduction reaction time, suggesting the increase of electron density

and the restoration of π-conjugated network within the graphene. Meanwhile, the peak at 300 nm gets disappeared, which further confirmed the graphitization of GO. These observations demonstrated that the reduction of GO had taken place. In other words, 1,2-diiodoethane could be used as a reducing agent for GO. The reduction mechanism may be attributed to the existence of hydrogen iodide coming from the elimination reaction of 1,2-diiodoethane under heating condition. *In situ* generated hydrogen iodide played an important role in the reduction process. As other studies have reported,[23, 24, 36] the possible reduction mechanism involves (a) ring-opening reaction of epoxide by iodide ions, resulting in hydroxyl groups and subsequent dehydration to the corresponding olefins, (b) nucleophilic substitution of hydroxyl group by iodide ions, and (c) elimination of iodide ions from the carbon lattice and restoration of graphene due to the weak binding energy of the carbon-iodide.

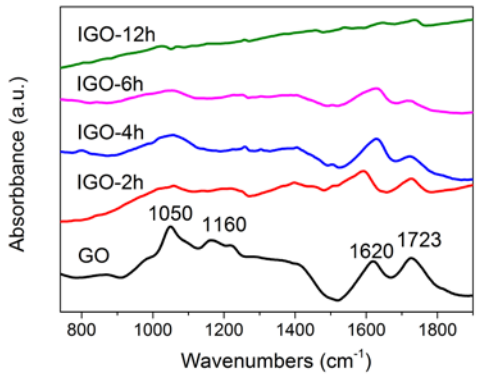

Fig. 3 FTIR spectra of GO and IGO with different reduction times.

The reduction of GO was also tracked by FT-IR spectroscopy. Fig. 3 shows the FTIR spectra of GO and IGO reduced by 1,2-diiodoethane in DMAc with different time intervals. In the case of GO, the characteristic peaks at 1723 cm^{-1}, 1620 cm^{-1}, 1160 cm^{-1} and 1050 cm^{-1} can be ascribed to C=O (ketone or carboxyl), C=C (unoxidized C-C bones), C-O-C (epoxide) and C-OH (alcoholic hydroxyl), respectively.[37, 38] These peaks illuminated that the GO contained abundant oxygen functional groups at the GO nanosheets. However, the spectra of IGO show a gradual decrease in the C=O peak with an increase of the reduction time, which could confirm the reduction of GO. Besides, the decrease in the intensities of the C-O-C peak over time was also observed. These observations indicated that most oxygen-containing groups on the GO sheets were removed due to the reduction of 1,2-diiodoethane.

The reduction of GO using 1,2-diiodoethane was further confirmed by X-ray diffraction (XRD) analysis. Flake graphite shows a very strong and sharp peak (002) at 2θ = 26.7° with the interlayer distance of 0.33 nm by Bragg's formula (Fig. 4). Compared with graphite, the pattern of GO exhibits a new strong peak at 10.7° assigning to *d*-spacing of 0.83 nm, which indicated that the lamellar structures of graphite had been destroyed and oxygen-containing groups had been inserted into the interspaces. With the reduction time extending, the peak at 10.7° gradually reduce, until it disappears completely when the reaction time reached 12 h, while a new diffraction peaks has appeared at about 25.0°, corresponding to the (002) planes of IGO, which was due to the removal of the oxygen-containing groups from GO sheets and restoration of a small amount of graphite structure.[39]

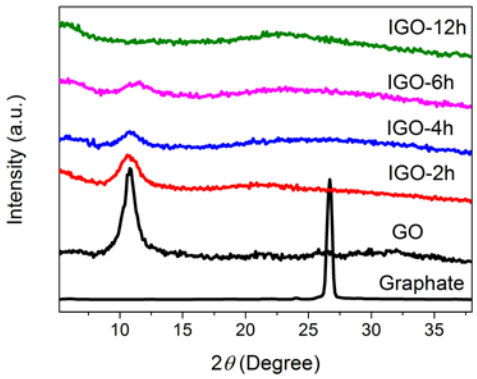

Fig. 4 XRD patterns of GO and IGO with different reduction times.

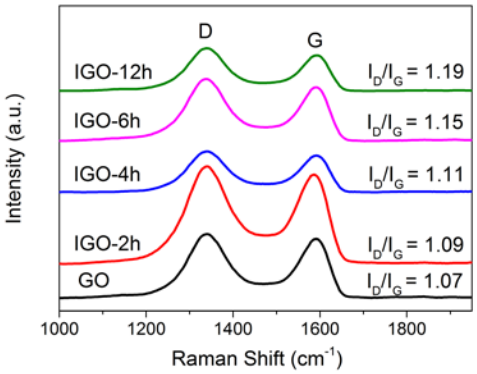

Fig. 5 Raman spectra of GO and IGO with different reduction times.

Raman spectroscopy was utilized to assess the structural and electronic conjugation states of GO and IGO. As illustrated in Fig. 5, the raman spectrum of GO exhibits two major features: 1339 cm^{-1} (D band) and 1591 cm^{-1} (G band), related to structural defects and partially disordered structures of sp^2 domains and E2g vibration mode of ordered sp^2 carbon atoms, respectively.[40] Thus the variation of conjugated electron state of graphene can be reflected by the change of the intensity ratio of the D band to the G band (I_D/I_G). The I_D/I_G ratio for GO was 1.07, however, the I_D/I_G ratio for IGO were increased gradually until 1.19, which implied that IGO had substantially high degree of disorder. The main reason lay in the oxygen-containing groups between the GO sheets were removed and the produced graphene structures aggregated randomly during the reduction.[41]

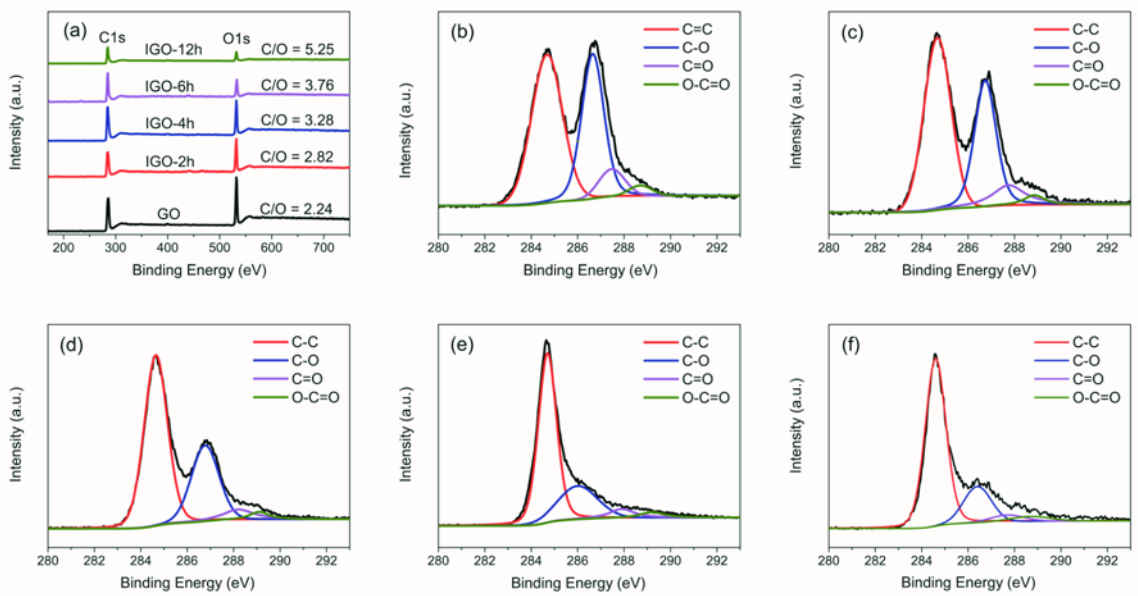

Fig. 6 (a) XPS survey spectra of GO and IGO with different reduction times, deconvoluted C 1s spectra of (b) GO, (c) IGO-2h, (d) IGO-4h, (e) IGO-6h, and (f) IGO-12h.

It is generally known that the reduction of GO means the elimination of oxygen-containing groups and the conversion of sp^3 bonds into sp^2 bonds. To evaluate the reduction extent of GO with 1,2-diiodoethane, XPS is used for the quantitative analysis of the surface elemental composition, and chemical and electronic states of the GO and IGO. The increase of C/O atomic ratio is an important evidence of GO reduction. In our experiment, the surface C/O atomic ratio of the IGO was increased from 2.24 to 5.25 with the increase of reducing time (Fig. 6(a)). Compared with the surface C/O atomic ratio of graphene reduced by hydrazine hydrate (10.2),[20] and hydroiodic acid (> 12),[23] the C/O atomic ratio using 1,2-diiodoethane as reducing reagent was relatively lower, however, which was comparable to that of using potassium iodide/hydrochloric acid (5.284)[25]. This suggested that 1,2-diiodoethane could serve as a effective reducing agent to implement the controllable transformation of GO to IGO under moderate reaction conditions without the addition of strong acid. Fig. 6(b-f) shows the deconvoluted spectra of GO, IGO-2h, IGO-4h, IGO-6h, and IGO-12h. The C1s spectrum of GO (Fig. 6b) displayed four peaks centered 284.7, 286.7, 287.5 and 288.8 eV, corresponding to the following functional groups: unoxidized graphite carbon sp^2 (C=C), epoxy/ hydroxyls (C-O), carbonyl (C=O) and carboxylate (O-C=O), respectively. It was obvious that the intensity of the peaks associated with oxygen-containing groups, especially the peak of C-O, decreased dramatically with the reduction time prolonging (Fig. 6(b-f)), which revealed that the oxygen-containing groups were gradually removed with the increase of the reduction extent.[42]

3.2. Electrical conductivity analysis of GO and IGO

The reduction of GO is more directly borne out by its enhanced electrical conductivity.[43] Fig. 7 shows the dependence of the electrical conductivities of graphene on reduction time. The conductivity of GO is 1.5×10^{-6} S m^{-1} which is regarded as an insulator due to insufficient of π-conjugation. However, the conductivity of IGO is gradually enhanced with the increase of reduction time. Especially, the conductivity of IGO-12h reaches 1.3×10^{2} S m^{-1}, which is nearly eight orders of magnitude higher than that of GO. In the view, the reducibility of 1,2-diiodoethane in DMAc may be comparable to that of sodium borohydride in water.[22, 44, 45] This was mainly attributed to the transformation of sp^3-hybridized carbon to sp^2 of IGO after reduction, which resulted in the restoration of π-electronic conjugation system.[46, 47] The higher conductivities of IGO further confirmed the higher reduction efficiency of 1,2-diiodoethane. As-prepared IGO sheets could be developed for a wider scope of applications in technology fields since 1,2-diiodoethane is safer, facile, controllable and environmentally friend. More importantly, 1,2-diiodoethane is a hydrophobic organic reducing agent, which can be compatible with most polymers. Therefore, 1,2-diiodoethane can be used as an ideal reducing agent for the fabrication of graphene-based polymer composites via *in situ* chemical reduction, particularly, for those (such as polyimide), which are sensitive to hydrazine.[48]

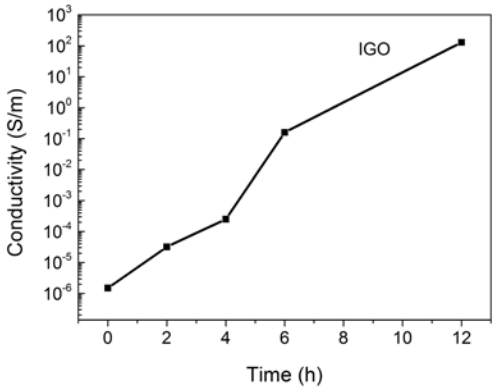

Fig.7 Electrical conductivities of IGO with different reduction times.

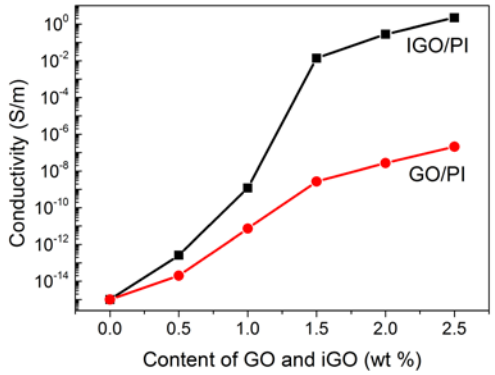

Fig. 8 Electrical conductivities of GO/PI films and IGO/PI films with different filler contents.

3.3. Electrical properties of GO/PI films and IGO/PI films

To demonstrate that the GO can be *in situ* reduced to IGO by 1,2-diiodoethane during the processing of polymerization, polyimide (PI) is used as the matrix of composites, which is recognized as one of the most important heat-resistant polymeric materials due to their overall balance of excellent temperature resistance, high intensity, strong toughness and good dimensional stability.[49]

Compared with the graphene, GO is potentially beneficial for the interactions with PAA, since GO possesses more functional groups on the surface of the sheets. Therefore, the solution of GO/PAA was firstly prepared via *in situ* polymerization of ODA and BPDA in GO dispersion in DMAc.[50] Afterwards, 1,2-diiodoethane was added to the solution of GO/PAA, followed by heat-induced gelatinization and imidization during which the stable dispersed GO was *in situ* reduced to IGO by 1,2-diiodoethane (Fig. 1). Consequently, the IGO/PI nanocomposite films were fabricated via ISCR. Fig. 8 presents the plots of electrical conductivity versus filler content for GO/PI and IGO/PI composites, respectively. Pure PI is a highly insulating material with an extremely low conductivity of 1.0×10^{-15} S m^{-1}. The conductivities of the composite films continue to increase with the increase of filler contents. The conductivities of the GO/PI composite films show corresponding increase from 2.0×10^{-14} to 2.1×10^{-7} S m^{-1} with 0.5 - 2.5 wt% GO. This could be ascribed to higher conductivity of the GO sheets (1.5×10^{-6} S m^{-1}) in comparison to pure PI. However, even the loading of 2.5 wt%, the conductivity of the GO/PI composite only is 2.1×10^{-7} S m^{-1}, which was considered to be insufficient for many practical applications. The most likely reason was that GO nanosheets cannot form a conductive network due to electrical insulation of GO. In the contrast, the conductivities for IGO/PI composites show considerable improvement. As compared with that of GO/PI, a sharp increase up to 1.4×10^{-2} S m^{-1} was observed with a small IGO content of 1.5 wt%. It was believed that the conductive network to produce a charge transport path throughout the insulating PI matrix had been constructed at 1.5 wt % IGO loading, which could be regarded as the percolation threshold.[51] The percolation threshold largely depends on large aspect ratio, better dispersion and high conductivity of IGO. With the increase of IGO content, the conductivity of IGO/PI further increases to 2.2 S m^{-1} at a 2.5 wt% IGO loading, which are nearly 10^7 times higher than that of the GO/PI composites at the same loading.

High conductivity of IGO/PI composites provided the direct evidence to the ISCR reaction of GO dispersed in polyimide matrix. This was mainly due to the fact that the processing temperature of the polyimide-based composites was enough to the ISCR reaction, by which the higher conductivity IGO was formed. Hence, the conductivities of IGO/PI composites via the ISCR reaction were higher than the results in some previous reports, which was not only higher than that of direct addition of functionalized graphene nanosheets into PI matrix (6.6×10^{-2} S m^{-1} at 3.0 wt%),[52] but also was higher than that of using the *in situ* thermal reduction method (3.0×10^{-2} S m^{-1} at 3.0 wt%),[53] and the *in situ* thermo-chemical reduction method (8.7×10^{-1} S m^{-1} at 10 wt%).[30] The remarkable high electrical conductivity and low percolation value of the IGO/PI composites could be attributed to the following reasons: (1) GO sheets could be well dispersed into PI matrix by means of solution blending due to the abundant oxygen functional groups at the edges and basal planes of the GO sheets (2) the sp^2-hybrid carbon network of IGO sheets could be effectively restored after 1,2-diiodoethane reduction (3) the ISCR reaction during composite process was beneficial to inhibit aggregation of IGO in virtue of the high viscosity during PI gelatinizing, and then the good dispersion state of the GO nanosheets could be maintained in the resulting composites, which contributed to form the graphene conductive network in the composites.

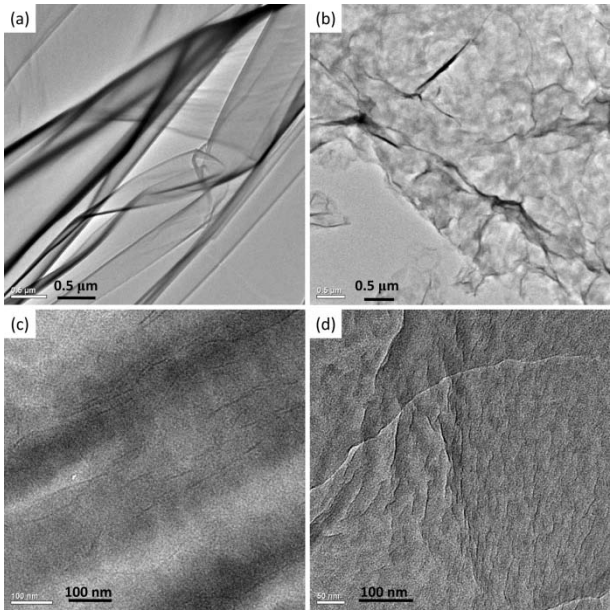

Fig. 9 TEM images of (a) GO (b) IGO-12h (c) 2.0 wt% GO/PI and (d) 2.0 wt% IGO/PI.

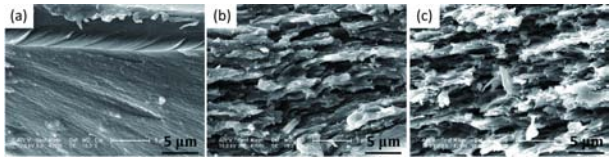

Fig. 10 SEM images of the fracture surfaces of (a) pure PI (b) 2.0 wt% GO/PI and (c) 2.0 wt% IGO/PI.

3.4. Morphological characterization

To obtain the micro-morphological information of GO and IGO in the dispersions, TEM observations are conducted, as shown in Fig. 9. The GO nanosheets have curled silk-like morphology with a lateral dimension of several micrometers (Fig. 9(a)). The typical crimp morphology was attributed to the disruption of the planar sp^2 structure by the introduction of sp^3-hybridized carbon upon oxidation.[41] After the reduction, the morphology of IGO sheets is distinctly different from that of GO. More folds or wrinkles were found in the TEM images of IGO (Fig. 9(b)). The shrinking nanosheets of IGO might originate from defective structures formed and its poor dispersibility in DMAc. Fig. 9(c) and (d) shows the dispersion of GO and IGO nanosheets in the ultrathin sections of 2.0 wt% GO/PI and 2.0 wt% IGO/PI composites, respectively. In GO/PI, the parallel dark lines structures represent the cross section of the GO layers (Fig. 9(c)). GO is dispersed well in the PI matrix as single or ultra-thin sheets with a thickness of less than several nanometers. The interfacial interactions between the oxygen-containing groups on the GO sheets and the PAA or PI matrix facilitated the exfoliation and dispersion of GO in the polymer matrix. As expected, IGO nanosheets are also well dispersed into PI matrix with a thickness of 1-10 nm. The good dispersion of IGO, as the aforementioned analysis, benefited from homogenously dispersion of the GO sheets in PI matrix and the *in situ* chemical reduction process which prevented GO from aggregating during its reduction. Such homogenous dispersion of IGO plays a key role in improving the electrical conductivity, mechanical properties and thermal stability of PI composites.

To further investigate the interfacial interaction between graphene and the PI matrix, the fracture surfaces of pure PI, 2.0 wt% GO/PI and 2.0 wt% IGO/PI films were observed by SEM upon tensile testing, as shown in Fig. 10. It is seen that the pure PI fracture surfaces exhibits a smooth surface, indicating typical brittle fracture characteristics. However, the fracture surfaces of 2.0 wt% GO/PI and 2.0 wt% IGO/PI composites are remarkably different as compared with that of pure PI, as shown in Fig. 10(b) and 10(c). The fracture surfaces of the two composites are relatively rough, which indicated strong interfacial interaction between GO or IGO and PI, as well as good dispersion of GO or IGO in PI.

3.5. Mechanical and thermal properties of GO/PI films and IGO/PI films

As shown in Fig. 11, by embedding of either GO or IGO into the PI, the tensile properties of the composites are significantly increased with the filler contents increasing from 0.5 wt % to 2.5 wt %. For example, pure PI possesses a tensile strength of 108 MPa and a Young's modulus of 2.05 GPa, while the incorporation of 2.5 wt% GO enhance the tensile strength and Young's modulus to 178 MPa and 3.17 GPa, respectively, corresponding to increases by about 65% and 54% as compared with that of the pure PI, respectively. The reinforcement effect of GO sheets for mechanical properties could be mainly attributed to its abundant oxygen functional groups at the sheets. These oxygen functional groups could enhance the filler-matrix non-covalent interaction (e.g., van der Waals attraction force or hydrogen bonding) and improve the GO dispersion in PI, which were in favour of stress transfer from the polymer matrix to GO sheets. Not surprisingly, the incorporation of IGO sheets also enhanced the tensile strength and Young's modulus of the composites, whereas, the extent of enhancement of IGO sheets for mechanical properties was slightly less than that of GO. With an IGO content of 2.5 wt%, the tensile strength, Young's modulus of the IGO/PI composites are increased by about 43% and 52% as compared with that of the pure PI, respectively (Fig. 11). Again, the improvement of mechanical properties was attributed to the presence of the non-covalent interaction between the remaining functional groups of IGO surfaces and PI matrix. However, the decrease of polar functional groups on the IGO surface after being reduced might weaken interfacial adhesion between the matrix and the reinforcements.[54, 55] Meanwhile, the improved mechanical properties of the IGO/PI may imply that the incorporation of 1,2-diiodoethane had little effect on the polyimide even though GO was effectively reduced by 1,2-diiodoethane. The reason lay probably in the escape of 1,2-diiodoethane and its decomposition products (hydrogen iodide, iodine, alkene or alkyne) from the composites during higher temperature process (350°C).

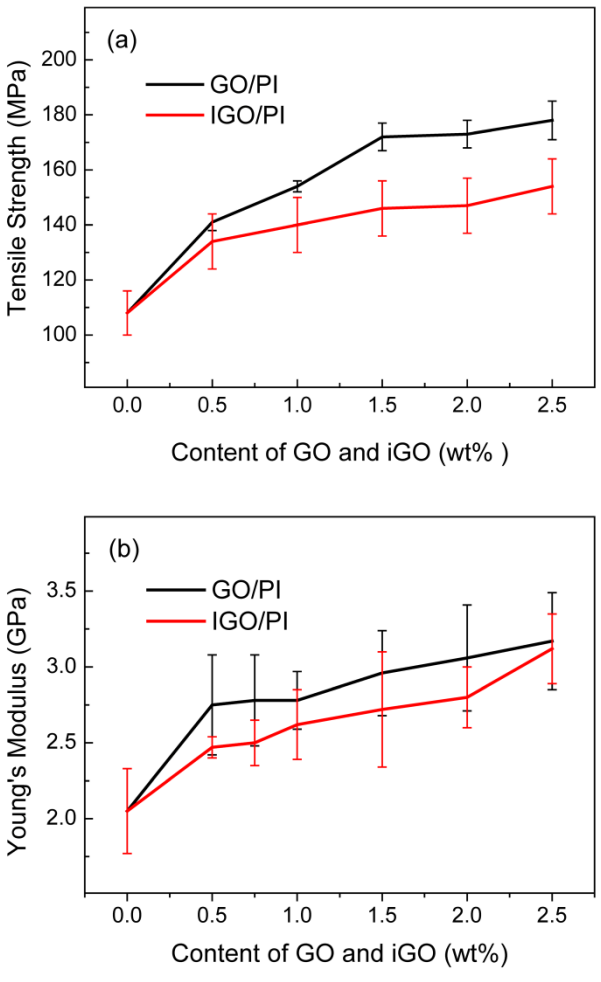

Fig. 11 Tensile properties of (a) GO/PI films and (b) IGO/PI films with different filler contents

The thermal stability is one of the most important properties for PI-based composites in high temperature applications. Fig. 12

illustrates the TGA traces of GO/PI and IGO/PI composite films. The incorporation of GO or IGO into the composites improved slightly thermal stability. Moreover, the degradation behaviour of the GO/PI nanocomposites was almost identical to that of IGO/PI nanocomposites. Since the thermal degradation of polymer originates from chain cleavage and radical formation, both the free radical scavenging and gas barrier effects of graphene in the nanocomposites might delay thermal degradation, and thereby, lead to improving thermal stability of the composites.[56] In addition, although thermally labile oxygen functional groups of GO sheets may be removed partially during *in situ* reduction and heat imidization, the remaining functional groups on graphene surface were enough to improve the filler-matrix interaction, and hence enhanced the thermal stability of the composites.

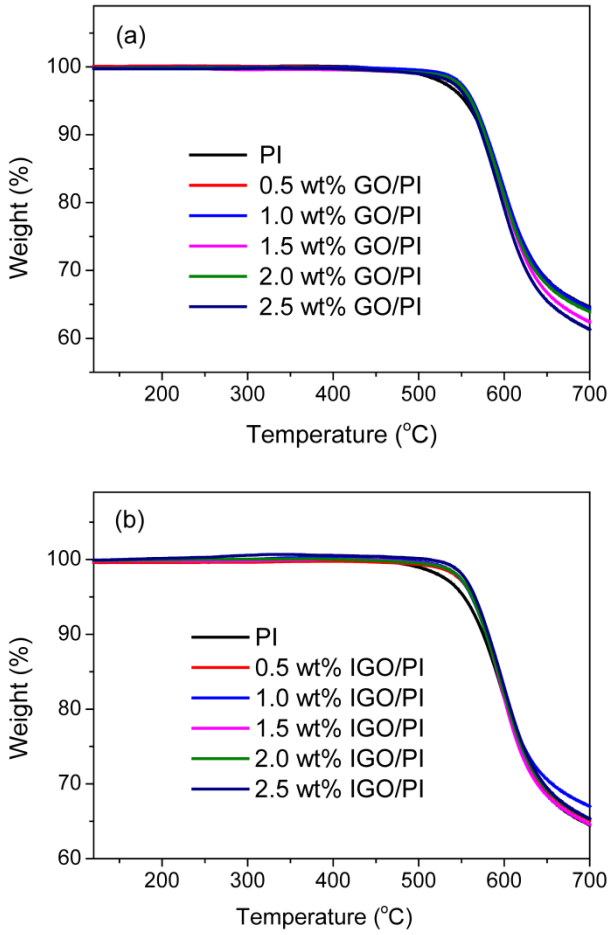

Fig.12 TGA profiles of (a) GO/PI films and (b) IGO/PI films with different filler contents

4. Conclusions

In summary, we developed an easy and effective approach for the fabrication of conductive graphene/polyimide composites via ISCR using 1,2-diiodoethane as the reducing agent. The composite films have high conductivity, as well as improved mechanical performances and thermal stability, which may benefit from the combination of dispersibility of GO in polymer matrix, high conductibility of IGO and high viscosity during heat-induced composites process. Furthermore , the introduction of 1,2-diiodoethane had virtually no influence on the polyimide, which indicated that 1,2-diiodoethane and its decomposition products might not remain in the composites. Hence, the ISCR-based fabrication methodology for conductive polymer composites can extend to other polymer composites in virtue of the heat process of composites.

Acknowledgements

This work was supported by the National Natural Science Foundation of China (51373164, 51233001) and the National High Technology Research and Development Program of China (2012AA03A211). We thank Professor Wenke Zhang (Jilin University) for valuable suggestions and Professor Shuping Xu (Jilin University) for kind assistance with raman measurements.

References

1. K. S. Novoselov, A. K. Geim, S. V. Morozov, D. Jiang, Y. Zhang, S. V. Dubonos, I. V. Grigorieva and A. A. Firsov, *Science*, 2004, **306**, 666-669.
2. K. S. Novoselov, A. K. Geim, S. V. Morozov, D. Jiang, M. I. Katsnelson, I. V. Grigorieva, S. V. Dubonos and A. A. Firsov, *Nature*, 2005, **438**, 197-200.
3. C. Lee, X. Wei, J. W. Kysar and J. Hone, *Science*, 2008, **321**, 385-388.
4. Z. Y, T. YW, S. HL and K. P, *Nature*, 2005, **438**, 201-204.
5. M. Jannik C, G. A K, K. M I, N. K S, B. T J and R. S, *Nature*, 2007, **446**, 60-63.
6. Z. Yanwu, M. Shanthi, C. Weiwei, L. Xuesong, S. J. Won, J. R. Potts and R. S. Ruoff, *Advanced Materials*, 2010, **22**, 3906-3924.
7. X. Wu, F. Tian, W. Wang, J. Chen, M. Wu and J. X. Zhao, *Journal of Materials Chemistry C*, 2013, **1**, 4676-4684.
8. M. S. Kang, K. T. Kim, J. U. Lee and W. H. Jo, *Journal of Materials Chemistry C*, 2013, **1**, 1870-1875.
9. W. J. Choi, Y. J. Chung, S. Myung, J. O. Lee, W. J. Min, W. Song, D. S. Jung, S. L. Sun, J. Lim and C. Y. Park, *Journal of Materials Chemistry C*, 2014, **24**, 4759-4763.
10. K. Rana, J. Singh and J.-H. Ahn, *Journal of Materials Chemistry C*, 2014, **2**, 2646-2656.
11. R. Sengupta, M. Bhattacharya, S. Bandyopadhyay and A. K. Bhowmick, *Progress in Polymer Science*, 2011, **36**, 638-670.
12. S. R. Dhakate, K. M. Subhedar and B. P. Singh, *Rsc Advances*, 2015, **5**, 43036-43057.
13. N. Yousefi, X. Sun, X. Lin, X. Shen, J. Jia, B. Zhang, B. Tang, M. Chan and J. K. Kim, *Adv Mater*, 2014, **26**, 5480-5487.
14. Q. Zhang, Y. Di, C. M. Huard, L. J. Guo, J. Wei and J. Guo, *Journal of Materials Chemistry C*, 2015, **3**, 1528-1536.
15. Z. Wang, S. Eigler, Y. Ishii, Y. Hu, C. Papp, O. Lytken, H.-P. Steinruck and M. Halik, *Journal of Materials Chemistry C*, 2015, **3**, 8595-8604.
16. J. Kiyoung, L. Taemin, C. Hyun Jung, P. J. Hyun, L. D. Jun, L. D. Wook and K. Byeong-Su, *Langmuir*, 2011, **27**, 2014-2018.
17. G. Yang and F. Zhao, *Journal of Materials Chemistry C*, 2014, **2**, 10201-10208.

18. S. Gambhir, R. Jalili, D. L. Officer and G. G. Wallace, *Npg Asia Materials*, 2015, **7**.
19. C. K. Chua and M. Pumera, *Chem Soc Rev*, 2014, **43**, 291-312.
20. S. Park, J. An, J. R. Potts, A. Velamakanni, S. Murali and R. S. Ruoff, *Carbon*, 2011, **49**, 3019-3023.
21. A. Ambrosi, C. K. Chua, A. Bonanni and M. Pumera, *Chemistry of Materials*, 2012, **24**, 2292-2298.
22. H.-J. Shin, K. K. Kim, A. Benayad, S.-M. Yoon, H. K. Park, I.-S. Jung, M. H. Jin, H.-K. Jeong, J. M. Kim, J.-Y. Choi and Y. H. Lee, *Advanced Functional Materials*, 2009, **19**, 1987-1992.
23. S. Pei, J. Zhao, J. Du, W. Ren and H.-M. Cheng, *Carbon*, 2010, **48**, 4466-4474.
24. C. Liu, F. Hao, X. Zhao, Q. Zhao, S. Luo and H. Lin, *Sci Rep*, 2014, **4**, 3965.
25. A. K. Das, M. Srivastav, R. K. Layek, M. E. Uddin, D. Jung, N. H. Kim and J. H. Lee, *J. Mater. Chem. A*, 2014, **2**, 1332-1340.
26. H. Zhao, Z. Peng, W. Wang, X. Chen, J. Fang and J. Xu, *Journal of Power Sources*, 2014, **245**, 529-536.
27. P. K. Mural, M. Sharma, G. Madras and S. Bose, *Rsc Advances*, 2015, **5**, 32078-32087.
28. L. Cui, X. Lu, D. Chao, H. Liu, Y. Li and C. Wang, *physica status solidi (a)*, 2011, **208**, 459-461.
29. N. Yousefi, X. Lin, Q. Zheng, X. Shen, J. R. Pothnis, J. Jia, E. Zussman and J.-K. Kim, *Carbon*, 2013, **59**, 406-417.
30. O. K. Park, M. G. Hahm, S. Lee, H. I. Joh, S. I. Na, R. Vajtai, J. H. Lee, B. C. Ku and P. M. Ajayan, *Nano Lett*, 2012, **12**, 1789-1793.
31. F.-Y. Yuan, H.-B. Zhang, X. Li, H.-L. Ma, X.-Z. Li and Z.-Z. Yu, *Carbon*, 2014, **68**, 653-661.
32. X. Zhao, Y. Li, J. Wang, Z. Ouyang, J. Li, G. Wei and Z. Su, *ACS Appl Mater Interfaces*, 2014, **6**, 4254-4263.
33. M. Sangermano, A. Tagliaferro, D. Foix, M. Castellino and E. Celasco, *Macromolecular Materials and Engineering*, 2014, **299**, 757-763.
34. J. William S. Hummers, Richard E. Offeman, *J Am Chem Soc*, 1958, **80**, 1339.
35. K. Kakaei and K. Hasanpour, *Journal of Materials Chemistry A*, 2014, **2**, 15428-15436.
36. I. K. Moon, J. Lee, R. S. Ruoff and H. Lee, *Nat Commun*, 2010, **1**, 73.
37. Q. Ma, J. Song, C. Jin, Z. Li, J. Liu, S. Meng, J. Zhao and Y. Guo, *Carbon*, 2013, **54**, 36-41.
38. Z. C, G. S, F. Y and D. S, *Acs Nano*, 2010, **4**, 2429-2437.
39. L. Xu, G. Xiao, C. Chen, R. Li, Y. Mai, G. Sun and D. Yan, *J. Mater. Chem. A*, 2015, **3**, 7498-7504.
40. X. Diez-Betriu, S. Alvarez-Garcia, C. Botas, P. Alvarez, J. Sanchez-Marcos, C. Prieto, R. Menendez and A. de Andres, *Journal of Materials Chemistry C*, 2013, **1**, 6905-6912.
41. J. Ning, J. Wang, X. Li, T. Qiu, B. Luo, L. Hao, M. Liang, B. Wang and L. Zhi, *Journal of Materials Chemistry A*, 2014, **2**, 10969-10973.
42. S. Obata, H. Tanaka and K. Saiki, *Carbon*, 2013, **55**, 126-132.
43. D. Luo, G. Zhang, J. Liu and X. Sun, *The Journal of Physical Chemistry C*, 2011, **115**, 11327-11335.
44. R. Ramachandran, M. Saranya, V. Velmurugan, B. P. C. Raghupathy, S. K. Jeong and A. N. Grace, *Applied Energy*, 2015, **153**, 22-31.
45. M. J. Fernández-Merino, L. Guardia, J. I. Paredes, S. Villar-Rodil, P. Solís-Fernández, A. Martínez-Alonso and J. M. D. Tascón, *J.phys.chem.c*, 2010, **114**, 6426-6432.
46. D. R. Dreyer, S. Park, C. W. Bielawski and R. S. Ruoff, *Chem Soc Rev*, 2010, **39**, 228-240.
47. W. Gao, L. B. Alemany, L. Ci and P. M. Ajayan, *Nat Chem*, 2009, **1**, 403-408.
48. J. Yan, Z. Wang, L. Gao and M. Ding, *Macromolecules*, 2006, **39**, 7555-7560.
49. M. Ding, *Progress in Polymer Science*, 2007, **32**, 623-668.
50. D. Chen, H. Zhu and T. Liu, *ACS Appl Mater Interfaces*, 2010, **2**, 3702-3708.
51. H. Deng, L. Lin, M. Ji, S. Zhang, M. Yang and Q. Fu, *Progress in Polymer Science*, 2014, **39**, 627-655.
52. O.-K. Park, J.-Y. Hwang, M. Goh, J. H. Lee, B.-C. Ku and N.-H. You, *Macromolecules*, 2013, **46**, 3505-3511.
53. C. Heo and J.-H. Chang, *Solid State Sciences*, 2013, **24**, 6-14.
54. L. Shao, J. Li, Y. Zhang, S. Gong, H. Zhang and Y. Wang, *Journal of Materials Chemistry A*, 2014, **2**, 14173-14183.
55. X. Zhao, Q. Zhang, D. Chen and P. Lu, *Macromolecules*, 2010, **43**, 2357-2363.
56. M. Tang, W. Xing, J. Wu, G. Huang, K. Xiang, L. Guo and G. Li, *J. Mater. Chem. A*, 2015, **3**, 5942-5948.

Graphical abstracts

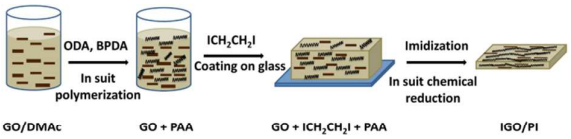

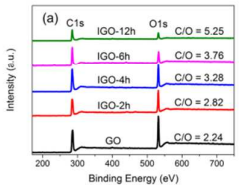

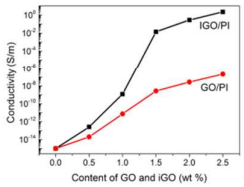

Graphene/polyimide composites with the conductivity of 2.22 S m^{-1} were fabricated via *in situ* reduction of graphene oxide by 1,2-diiodoethane.